# The First Transmembrane Segment of the Dopamine D2 Receptor: Accessibility in the Binding-Site Crevice and Position in the Transmembrane Bundle

Lei Shi,[‡,§] Merrill M. Simpson,[‡] Juan A. Ballesteros,[||] and Jonathan A. Javitch*[,‡,§,⊥]

*Center for Molecular Recognition and Departments of Pharmacology and Psychiatry, College of Physicians and Surgeons, Columbia University, 630 West 168th Street, New York, New York 10032, and Novasite Pharmaceuticals, Inc., 3520 Dunhill Street, San Diego, California 92121*

*Received June 12, 2001; Revised Manuscript Received August 3, 2001*

ABSTRACT: The binding site of the dopamine D2 receptor, like that of homologous G-protein-coupled receptors (GPCRs), is contained within a water-accessible crevice formed among its seven transmembrane segments (TMs). Using the substituted-cysteine-accessibility method (SCAM), we are mapping the residues that contribute to the surface of this binding-site crevice. We have now mutated to cysteine, one at a time, 21 consecutive residues in TM1. Six of these mutants reacted with charged sulfhydryl reagents, whereas bound antagonist only protected N52$^{1.50}$C from reaction. Except for A38$^{1.36}$C, none of the substituted cysteine mutants in the extracellular half of TM1 appeared to be accessible. Pro$^{1.48}$ is highly conserved in opsins, but absent in catecholamine receptors, and the high-resolution rhodopsin structure showed that Pro$^{1.48}$ bends the extracellular portion of TM1 inward toward TM2 and TM7. Analysis of the conversation of residues in the extracellular portion of TM1 of opsins showed a pattern consistent with α-helical structure with a conserved face. In contrast, this region in catecholamine receptors is poorly conserved, suggesting a lack of critical contacts. Thus, in catecholamine receptors in the absence of Pro$^{1.48}$, TM1 may be straighter and therefore further from the helix bundle, consistent with the apparent lack of conserved contact residues. When examined in the context of a model of the D2 receptor, the accessible residues in the cytoplasmic half of TM1 are at the interface with TM7 and with helix 8 (H8). We propose the existence of critical contacts of TM1, TM7, and H8 that may stabilize the inactive state of the receptor.

The binding sites of amine G-protein-coupled receptors (GPCRs)[1] are formed among their seven transmembrane segments (TMs) (*1*) and are accessible to charged, water-soluble agonists, like dopamine. Thus, for each of these receptors, the binding site is contained within a water-accessible crevice, the binding-site crevice, which extends from the extracellular surface of the receptor into the transmembrane domain. The surface of this crevice is formed by residues that can contact specific agonists and/or antagonists and by other residues that may play a structural role and affect binding indirectly.

Despite an enormous amount of research on the structure and function of these receptors, until very recently no high-resolution structure of any GPCR was available. Inferences about the structure of these receptors have been based on cryomicroscopy studies of rhodopsin that gave an indication of the relative disposition of the seven TMs (*2*). Molecular models of rhodopsin and other GPCRs have been built based on this low-resolution structure, on additional experimental data pertinent to structure, and on inferences from sequence alignments, analyzed in terms of conservation and physicochemical properties (*3*−*5*). In the initial projection map for rhodopsin, TM1 appeared somewhat remote from the binding site, and TM1 has not received extensive consideration as a contributor to ligand binding. The limited number of mutagenesis experiments in amine receptors has not identified any residues involved in ligand binding or ligand specificity (*6*). Studies of chemokine receptors have even suggested that TM3 to TM7 can be a functional unit without TM1 and TM2 (*7*). In the bradykinin B2 receptor, the loop between TM1 and TM2 appeared to be accessible to extracellular reagents, suggesting that the topology of this region may not be strictly conserved or that this region may be very dynamic (*8*). The high-resolution structure of bovine rhodopsin (*9*) confirmed and refined the structure inferred from the earlier cryomicroscopy studies and showed TM1 to be the most peripheral TM relative to the transmembrane bundle and the TM1−TM2 loop to be intracellular.

Here we report the application of the substituted-cysteine-accessibility method (SCAM) to identify systematically residues in TM1 (Ala38$^{1.36}$−Val59$^{1.57}$) of the dopamine D2

[†] This work was supported by NIH Grants MH57324 and MH54137, by the G. Harold & Leila Y. Mathers Charitable Trust, by the Lebovitz Trust, and by the Lieber Center.

* Corresponding author. Email: jaj2@columbia.edu; Phone: 212-305-7308; Fax: 212-305-5594.

[‡] Center for Molecular Recognition, Columbia University.

[§] Department of Pharmacology, Columbia University.

[||] Novasite Pharmaceuticals, Inc.

[⊥] Department of Psychiatry, Columbia University.

[1] Abbreviations: GPCRs, G-protein-coupled receptors. TM, transmembrane segment; TM*X*, the *X*th transmembrane segment; SCAM, substituted-cysteine-accessibility method; MTS, methanethiosulfonate; MTSEA, MTSethylammonium; MTSET, MTSethyltrimethylammonium; MTSES, MTSethylsulfonate; MTSHTEA, MTShexyltrimethylammonium.

10.1021/bi011204a CCC: $20.00 
Published on Web 09/22/2001

receptor that contribute to the binding-site crevice. We have used SCAM (*10*, *11*) to identify the residues in TM2, TM3, TM4, TM5, TM6, and TM7 that form the surface of the binding-site crevice in the human dopamine D2 receptor (*12*−*18*). Consecutive residues in the TMs are mutated to cysteine, one at a time, and the mutant receptors are expressed in heterologous cells. If ligand binding to a cysteine-substitution mutant is near-normal, we assume that the structure of the mutant receptor, especially around the binding site, is similar to that of wild type and that the substituted cysteine lies in a similar orientation to that of the wild-type residue. In the TMs, the sulfhydryl of a cysteine facing into the binding-site crevice should react much faster with charged sulfhydryl-specific reagents than should sulfhydryls facing into the interior of the protein or into the lipid bilayer. For such reagents, we use derivatives of methanethiosulfonate (MTS): positively charged MTSethylammonium (MTSEA) and MTSethyltrimethylammonium (MTSET), and negatively charged MTSethylsulfonate (MTSES) (*19*). These reagents are about the same size as dopamine, with maximum dimensions of approximately 10 Å by 6 Å. They form mixed disulfides with the cysteine sulfhydryl, covalently linking $-SCH_2CH_2X$, where X is $NH_3^+$, $N(CH_3)_3^+$, or $SO_3^-$. We use two criteria for identifying an engineered cysteine as forming the surface of the binding-site crevice: (i) the reaction with an MTS reagent alters binding irreversibly; (ii) this reaction is retarded by the presence of ligand. The SCAM analysis is presented here in the context of results from sequence analysis and molecular representation/modeling of TM1 based on the bovine rhodopsin high-resolution structure (*9*).

## EXPERIMENTAL PROCEDURES

*Numbering of Residues*. Residues are numbered according to their positions in the human dopamine D2 receptor sequence. We also index residues relative to the most conserved residue in the TM in which it is located (*4*). By definition, the most conserved residue is assigned the position index "50", e.g., Asn52$^{1.50}$, and therefore Gly51$^{1.49}$ and Val53$^{1.51}$. This indexing simplifies the identification of aligned residues in different GPCRs.

*Site-Directed Mutagenesis*. Cysteine mutations were generated as described previously (*17*). Mutations were confirmed by DNA sequencing. Mutants are named as (wild-type residue)(residue number)$^{\text{position index}}$(mutant residue), where the residues are given in the single-letter code.

*Transfection*. The cDNA encoding the human dopamine $D2_{short}$ receptor or the appropriate cysteine mutant, epitope-tagged at the amino terminus with the cleavable influenza−hemagglutinin signal-sequence followed by the "FLAG"-epitope (IBI, New Haven, CT) (*14*) in the bicistronic expression vector pcin4 (a gift from Dr. S. Rees, Glaxo) (*20*), was used for all transfections, which were performed as described previously (*14*).

HEK 293 cells in DMEM/F12 (1:1) with 10% bovine calf serum (Hyclone) were maintained at 37 °C and 5% $CO_2$. For stable transfection, 35 mm dishes of HEK 293 cells at 70−80% confluence were transfected with 2 μg of wild-type or mutant D2 receptor cDNA in pcin4 (see above) using 9 μL of lipofectamine (Gibco) and 1 mL of OPTIMEM (Gibco). Five hours after transfection, the solution was removed, and fresh media were added. Twenty-four hours after transfection, the cells were split to a 100 mm dish, and 700 μg/mL Geneticin was added to select for a stably transfected pool of cells.

*Harvesting Cells*. Cells were washed with phosphate-buffered saline (PBS: 8.1 mM $NaH_2PO_4$, 1.5 mM $KH_2PO_4$, 138 mM NaCl, 2.7 mM KCl, pH 7.2), briefly treated with PBS containing 1 mM EDTA, and then dissociated in PBS. Cells were pelleted at 1000*g* for 5 min at 4 °C, and resuspended for binding or treatment with MTS reagents.

[$^3$*H*]*N-Methylspiperone Binding*. Whole cells from a 35 mm plate were suspended by pipetting in 400 μL of buffer A (25 mM HEPES, 140 mM NaCl, 5.4 mM KCl, 1 mM EDTA, 0.006% BSA, pH 7.4). Cells were then diluted with buffer A, typically 20-fold. Depending on the level of expression in the various mutants, adjustments in the number of cells per assay tube were made as necessary to prevent depletion of ligand in the case of very high expression or to increase the signal in the case of low expression. [$^3$H]*N*-Methylspiperone (Dupont/NEN) binding was performed as described previously (*15*).

*Reactions with MTS Reagents*. Whole cells from a 35 mm plate were suspended in 400 μL of buffer A. Aliquots (45 μL) of cell suspension were incubated with freshly prepared MTS reagents (5 μL) at the stated concentrations at room temperature for 2 min. Cell suspensions were then diluted 16-fold, and 200 μL aliquots were used to assay for [$^3$H]*N*-methylspiperone (150 pM) binding as described (*15*). The fractional inhibition was calculated as: 1 − [(specific binding after MTS reagent)/(specific binding without reagent)]. We used SPSS for Windows (SPSS, Inc.) to analyze the effects of the MTS reagents by one-way ANOVA with Dunnett's post hoc test ($p < 0.05$).

The second-order rate constant ($k$) for the reaction of MTSEA with each susceptible mutant was estimated by determining the extent of reaction after a fixed time, 2 min, with six concentrations of MTSEA (typically 0.025−10 mM) (all in excess over the reactive sulfhydryls). The fraction of initial binding, $Y$, was fit to $(1 - \text{plateau})e^{-kct} + \text{plateau}$, where plateau is the fraction of residual binding at saturating concentrations of MTSEA, $k$ is the second-order rate constant (in $M^{-1}\ s^{-1}$), $c$ is the concentration of MTSEA (M), and $t$ is the time (120 s).

*Sequence Conservation and Periodicity Analysis*. The method used to calculate the conservation index (CI) was based on that of Visiers et al. (*3*), with modifications as described below. At a given position within a multiple sequence alignment, the number of different amino acid residues, the quantitative significance of pairwise substitution probabilities, and the frequency of appearance of each type of residue were integrated to quantitate the degree of conservation at that position.

The $N$ different residues that appear at a given position can be mapped to $N$ points in an $N - 1$ dimensional Euclidean space, in which $D_{xy}$ is the distance between point $x$ and point $y$. A Euclidean space implies (a) $D_{xy} = D_{yx}$ for any given pair of points, and (b) triangular inequality, $D_{xy} < (D_{xz} + D_{yz})$, for any given set of three points $x$, $y$, and $z$. The volume ($V$) of the simplex (the figure that in any given number of dimensions is bounded by the least possible number of hyperplanes) connected by these $N$ points is given by (*21*).

$$V = \sqrt{\frac{(-1)^N}{2^{N-1} \times ((N-1)!)^2} \times \begin{vmatrix} 0 & 1 & 1 & \cdots & 1 \\ 1 & 0 & D_{12}^2 & \cdots & D_{1N}^2 \\ 1 & D_{21}^2 & 0 & \cdots & D_{2N}^2 \\ \vdots & \vdots & \vdots & \ddots & \vdots \\ 1 & D_{N1}^2 & D_{N2}^2 & \cdots & 0 \end{vmatrix}}$$

With increasing $N$, $V$ decreases quickly; with decreasing $D$, $V$ also decreases. To let the distance $D$ between any pair of points represent the integrated probability of substituting one residue for other, we performed the following transformation. To satisfy (a), the following formula was developed to integrate $\Pi_{x\rightarrow y}$ (the probability of a mutation from residue $x$ to residue $y$) and $\Pi_{y\rightarrow x}$ from a substitution probability table specifically calculated for residues in α-helices (*22*), by considering the frequencies of appearance of a certain residue ($f_a$) at a given position:

$$\Pi_{xy} = \frac{f_x}{f_x + f_y} \times \Pi_{x\rightarrow y} + \frac{f_y}{f_x + f_y} \times \Pi_{y\rightarrow x}$$

According to the substitution probability table we used (*22*), triangular inequality was not satisfied for all possible sets of three points; therefore, two constants ($c_1$ and $c_2$) were introduced, where $D_{xy} = D_{yx} = c_1 + c_2\Pi_{xy}$. $c_1$ and $c_2$ were chosen empirically not only to satisfy triangular inequality, but also to increase the impact of $\Pi_{xy}$ by making $c_2/c_1$ as large as possible, while keeping the final $V$ equal to or less than 1. For the data set analyzed here, $c_1 = 0.67$ and $c_2 = 1.7$. Because $V$ is very sensitive to $N$, to reduce the impact of very rare sequences and/or potential errors in sequence or alignment, residues that appear at a given position with a frequency of less than 1% were not included in the calculation of $V$.

In a case where $N$ different residues are present, the frequency distribution of these residues, in addition to the value of $N$, also reflects an aspect of the degree of conservation, if the set of available sequences is adequately representative. Thus, a distribution of 98:1:1 is more conserved than a distribution of 40:30:30, even though three different residues are present in both cases. To give greater weight to the former situation, we calculated the information content (*23*) of each position, which is another measure of conservation:

$$I_i = \sum_{a \in A} f_{ia} \log_2 \frac{f_{ia}}{p_a}$$

where $A$ is the set of residues present at position $i$, and $p_a$ is the a priori distribution of the residues for the environmental and structural context (taken to be 0.05 for each of the 20 amino acids). The results were normalized by division by $\log_2(1/0.05)$.

To integrate these two scales, we took the average of $V$ and $I$ to be the conservation index (CI):

$$\mathrm{CI}_i = (V_i + I_i)/2$$

This algorithm was implemented with a Perl script and applied to a comparison between two multiple alignments (MA). One alignment was of 101 sequences of all known opsins with Pro at position 1.48 (rMA). The second alignment, which includes the dopamine D2 receptor, was of 104 sequences of all known catecholamine receptors with Gly at position 1.49 (cMA).

The discrete Fourier transform power spectra, $P(\omega)$ (*24*−*26*), was calculated as

$$P(\omega) = [\sum_{j=1}^{S} (\mathrm{CI}_j - \overline{\mathrm{CI}}) \cos(j\omega)]^2 + [\sum_{j=1}^{S} (\mathrm{CI}_j - \overline{\mathrm{CI}}) \sin(j\omega)]^2$$

where $S$ is the number of residues in the segment of sequence being analyzed, $\omega$ is the angular rotation angle between residues around an axis (100° for an ideal helix), and $\overline{\mathrm{CI}}$ is the mean value of CI for the entire sequence segment studied. The α-helical character of the $P(\omega)$ curve can be quantified as

$$\Psi = [(1/30)\int_{85^\circ}^{115^\circ} P(\omega)\, d\omega]/[(1/180)\int_{0^\circ}^{180^\circ} P(\omega)\, d\omega]$$

The greater the fraction of the $P(\omega)$ curve that is in the α-helical region (85°−115°), the greater the resulting Ψ (*25*).

*Molecular Modeling*. A human dopamine D2 receptor model was made based on the crystal structure of bovine rhodopsin (*9*). Initially, each transmembrane segment from TM2 to TM7 was modeled as described (*27*). TM1 of the dopamine D2 receptor does not contain a Pro at 1.48 as does rhodopsin, and we expected that the structures may diverge in this region. For reasons discussed below, we initially modeled TM1 of the D2 receptor as a straight helix. The conserved cytoplasmic portions of the simulated helices for each of the seven TMs were superimposed on the bovine rhodopsin backbone. The rotamers of the conserved residues were fixed to those of the aligned positions in the bovine rhodopsin structure. The remaining side chain rotamers were assigned initial values in a backbone-dependent manner by SCWRL (*28*). Energy minimization with CHARMM (version 27b1) (*29*) was used to relieve side chain clashes and to allow limited local structural effects on the backbone.

The D2 receptor and related catecholamine receptors contain a highly conserved Gly$^{1.49}$, and this residue may induce a certain degree of flexibility (*30*) and allow some extent of bend in TM1 of catecholamine receptors. To explore the bending of a membrane-spanning α-helix by glycine, an α-helix was created that contained 30 amino acids with a Gly at position 20 from the N-terminus and Ala at the other positions. The α-helix was capped by acetamide at the N-terminus and N-methylamide at the C-terminus, and ideal α-helix torsion angles ($\varphi = -65^\circ$, $\psi = -47^\circ$) were used for each residue. The structure was energy minimized, and the resulting structure was used in molecular dynamics (MD) simulations in CHARMM with the leap-frog algorithm in a hydrophobic environment (fixed dielectric constant of 4), and with constraints on bonds involving hydrogens by the SHAKE algorithm. The backbone dihedral angles (A) were restrained around the ideal α-helix angles (Min) by well shaped energy barriers [10° on each side (Width), force constant (Force) of 5 kcal/mol/radian$^2$; the energy of

Table 1: Characteristics of [$^3$H]*N*-Methylspiperone Binding to Cysteine-Substituted Dopamine D2 Receptor[a]

| mutant | $K_D$ (pM) | $K_{MUT}/K_{C118S}$ | $B_{MAX}$ (fmol/cm$^2$) |
|---|---|---|---|
| A38$^{1.36}$C | 56 ± 26 | 1.6 | 109 ± 16 |
| T39$^{1.37}$C | 86 ± 55 | 2.4 | 207 ± 37 |
| L40$^{1.38}$C | 76 ± 34 | 2.1 | 188 ± 4 |
| L41$^{1.39}$C | 64 ± 22 | 1.8 | 106 ± 7 |
| T42$^{1.40}$C | 64 ± 25 | 1.8 | 173 ± 5 |
| L43$^{1.41}$C | 70 ± 43 | 2.0 | 182 ± 2 |
| L44$^{1.42}$C | 58 ± 36 | 1.6 | 227 ± 14 |
| I45$^{1.43}$C | 32 ± 11 | 0.9 | 130 ± 43 |
| A46$^{1.44}$C | 20 ± 6 | 0.6 | 175 ± 57 |
| V47$^{1.45}$C | 19 ± 6 | 0.5 | 133 ± 44 |
| I48$^{1.46}$C | 64 ± 23 | 1.8 | 503 ± 111 |
| V49$^{1.47}$C | 25 ± 8 | 0.7 | 159 ± 53 |
| F50$^{1.48}$C | 74 ± 2 | 2.1 | 302 ± 49 |
| G51$^{1.49}$C | 76 ± 31 | 2.1 | 125 ± 12 |
| N52$^{1.50}$C | 41 ± 3 | 1.1 | 33 ± 2 |
| V53$^{1.51}$C | 86 ± 8 | 2.4 | 302 ± 7 |
| L54$^{1.52}$C | 36 ± 3 | 1.0 | 323 ± 31 |
| V55$^{1.53}$C | 59 ± 2 | 1.6 | 177 ± 6 |
| C56$^{1.54}$(C118$^{3.36}$S) | 36 ± 3 | 1.0 | 110 ± 2 |
| M57$^{1.55}$C | 49 ± 4 | 1.4 | 142 ± 4 |
| A58$^{1.56}$C | 168[b] ± 11 | 4.7 | 134 ± 8 |
| V59$^{1.57}$C | 35 ± 1 | 1.0 | 90 ± 4 |

[a] Data were fit to the binding isotherm by nonlinear regression. The means and SEM are shown for 2−3 independent experiments, each with duplicate determinations. $B_{MAX}$ values are presented as femtomoles per square centimeter of plate area. [b] $K_D$ was significantly different ($p < 0.05$) than that of C56$^{1.54}$(C118S) by one-way ANOVA and Dunnett's post hoc test.

constraint dihedral angle (Ecdih) was calculated by Ecdih = Force × max(0, abs(A − Min) − Width)$^2$]. During the MD simulations, the α-helix was heated from 0 K to 300 K over 12 picoseconds (ps). After a 100 ps equilibration phase and a 300 ps production phase, an average structure was calculated from the trajectory of the last 50 ps of simulation. The bend angle of the average structure was calculated according to (*31*).

## RESULTS

*Effects of Cysteine Substitution on Antagonist Binding*. In a background of the mutant C118$^{3.36}$S, which is relatively insensitive to the MTS reagents (*18*), we mutated to cysteine, one at a time, 21 residues, Ala38$^{1.36}$ to Val59$^{1.57}$, in TM1, which contains Cys56$^{1.54}$, an endogenous cysteine that was present in C118S and thus in all of the mutants. Each mutant receptor was stably expressed in HEK 293 cells, and the $K_D$ and $B_{MAX}$ characterizing the equilibrium binding of the radiolabeled antagonist, [$^3$H]*N*-methylspiperone, were determined. At 20 positions, the $K_D$ of the cysteine-substitution mutant was between 0.5 and 2.4 times the $K_D$ of C118S, and at A58$^{1.56}$C, the $K_D$ was 4.7 times that of C118S. At all 21 positions, the $B_{MAX}$ ranged from 30% to 460% of that obtained with C118S (Table 1). The $K_I$ of the antagonist sulpiride in competition with [$^3$H]*N*-methylspiperone was determined in the mutants (Table 2). The effects on sulpiride affinity were less than 3-fold at every position, except for L41$^{1.39}$C and for N52$^{1.50}$C, the affinities of which were 4.2- and 5.3-fold lower than wild type (Table 2).

*Reactions of Charged MTS Reagents with the Mutants*. A 2 min application of 2.5 mM MTSEA significantly inhibited [$^3$H]*N*-methylspiperone binding to 5 of 21 cysteine-substitution mutants (Figure 1). A 2 min application of 0.25 mM MTSEA did not significantly inhibit binding to any of these mutants (data not shown). To quantitate the susceptibility to MTSEA, we determined the second-order rate constants

Table 2: Inhibitory Potency of (−)-Sulpiride on [$^3$H]*N*-Methylspiperone Binding to Cysteine-Substituted Dopamine D2 Receptor[a]

| mutant | apparent $K_I$ (nM) | $K_{I(MUT)}/K_{I(C118S)}$ |
|---|---|---|
| A38$^{1.36}$C | 2.3 ± 0.3 | 1.4 |
| T39$^{1.37}$C | 3.1 ± 0.2 | 1.9 |
| L40$^{1.38}$C | 2.5 ± 0.2 | 1.5 |
| L41$^{1.39}$C | 7.0 ± 1.4 | 4.2 |
| T42$^{1.40}$C | 3.3 ± 0.2 | 2.0 |
| L43$^{1.41}$C | 1.3 ± 0.1 | 0.8 |
| L44$^{1.42}$C | 4.4 ± 0.3 | 2.6 |
| I45$^{1.43}$C | 1.6 ± 0.5 | 0.9 |
| A46$^{1.44}$C | 0.9 ± 0.1 | 0.5 |
| V47$^{1.45}$C | 0.7 ± 0.4 | 0.4 |
| I48$^{1.46}$C | 0.8 ± 0.2 | 0.5 |
| V49$^{1.47}$C | 2.4 ± 0.6 | 1.5 |
| F50$^{1.48}$C | 2.0 ± 0.5 | 1.2 |
| G51$^{1.49}$C | 4.2 ± 0.2 | 2.5 |
| N52$^{1.50}$C | 8.8[b] ± 3.4 | 5.3 |
| V53$^{1.51}$C | 2.9 ± 0.1 | 1.7 |
| L54$^{1.52}$C | 4.6 ± 1.7 | 2.8 |
| V55$^{1.53}$C | 2.4 ± 0.2 | 1.4 |
| C56$^{1.54}$(C118$^{3.36}$S) | 1.7 ± 0.1 | 1.0 |
| M57$^{1.55}$C | 2.2 ± 0.0 | 1.3 |
| A58$^{1.56}$C | 2.1 ± 0.3 | 1.3 |
| V59$^{1.57}$C | 2.3 ± 0.3 | 1.4 |

[a] Cells transfected with the appropriate receptor were assayed with [$^3$H]*N*-methylspiperone (150 pM) in the presence of nine concentrations of (−)-sulpiride. The apparent $K_I$ was determined by the method of Cheng and Prusoff using the $IC_{50}$ value obtained by fitting the data to a variable slope competition model by nonlinear regression. The means and SEM are shown for 2 independent experiments, each with duplicate determinations. [b] $K_I$ was significantly different ($p < 0.05$) than that of C56$^{1.54}$(C118S) by one-way ANOVA and Dunnett's post hoc test.

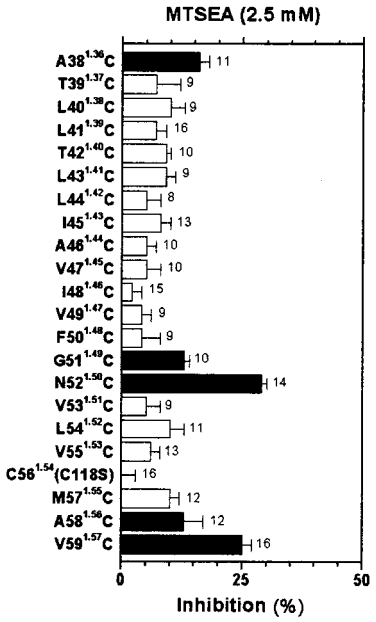


FIGURE 1: Inhibition of specific [$^3$H]*N*-methylspiperone (150 pM) binding to intact cells transfected with wild-type or mutant D2 receptors resulting from a 2 min application of 2.5 mM MTSEA. The means and SEM are shown. The number of independent experiments for each mutant is shown next to the bars. Solid bars indicate mutants for which inhibition was significantly different ($p < 0.05$) than C56$^{1.54}$(C118S) by one-way ANOVA and Dunnett's post hoc test.

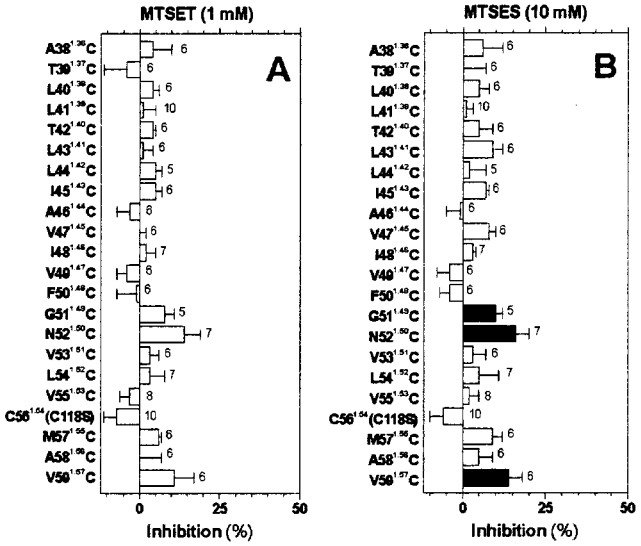


FIGURE 2: Inhibition of specific [$^3$H]*N*-methylspiperone (150 pM) binding to intact cells transfected with wild-type or mutant D2 receptors resulting from a 2 min application of (A) 1 mM MTSET or (B) 10 mM MTSES. Based on the relative rate constants for reaction with simple thiols in solution, namely, 10:4:1 for MTSET, MTSEA, and MTSES, we used equireactive concentrations of 1 mM MTSET, 2.5 mM MTSEA, and 10 mM MTSES. The means and SEM are shown. The number of independent experiments for each mutant is shown next to the bars. Solid bars indicate mutants for which inhibition was significantly different ($p < 0.05$) than C56$^{1.54}$(C118S) by one-way ANOVA and Dunnett's post hoc test.

for the reaction of MTSEA with N52$^{1.50}$C and with V159$^{1.57}$C, the two mutants for which the effect of reaction was large to allow such a determination. The rates of reaction were slow, with values of $2.8 \pm 0.4$ $M^{-1}$ $s^{-1}$ ($n = 4$) and $1.0 \pm 0.1$ $M^{-1}$ $s^{-1}$ ($n = 4$) for N52$^{1.50}$C and V59$^{1.57}$C, respectively. Due to the small effects on binding of the reaction of the mutants with MTSEA, protection experiments with the antagonist sulpiride were also only performed on N52$^{1.50}$C and V59$^{1.57}$C. Sulpiride significantly retarded the reaction of N52$^{1.50}$C ($43 \pm 9\%$, $n = 2$, $p < 0.05$) but not of V59$^{1.57}$C ($13 \pm 7\%$, $n = 2$, $p > 0.1$) with MTSEA.

Because TM1 is the furthest TM from the binding-site crevice and because we use effects on ligand binding as an indirect readout of reaction, there is a significant chance of false negative determinations of accessibility with MTSEA, MTSET, and MTSES in TM1. We reasoned that reaction of a substituted Cys with a MTS reagent that adds a longer and/or bulkier group to the sulfhydryl might impact more on subsequent ligand binding, although the hydrophobic nature of the spacer arm may complicate the determination of accessibility. The 2 min application of 0.25 mM MT-Shexyltriethylammonium (MTSHTEA) significantly inhibited [$^3$H]*N*-methylspiperone binding only to N52$^{1.50}$C and to V55$^{1.53}$C (data not shown).

At 10 mM, MTSES, a negatively charged MTS derivative, significantly inhibited a subset of the residues that reacted with MTSEA, G51$^{1.49}$C, N52$^{1.50}$C, and V59$^{1.57}$C (Figure 2). None of the mutants was significantly inhibited by treatment with 1 mM MTSET (Figure 2).

*Sequence Conservation and Periodicity Analysis.* The most conserved residue in TM1 of all rhodopsin-like GPCRs is the Asn at position 1.50. In opsins, there is a highly

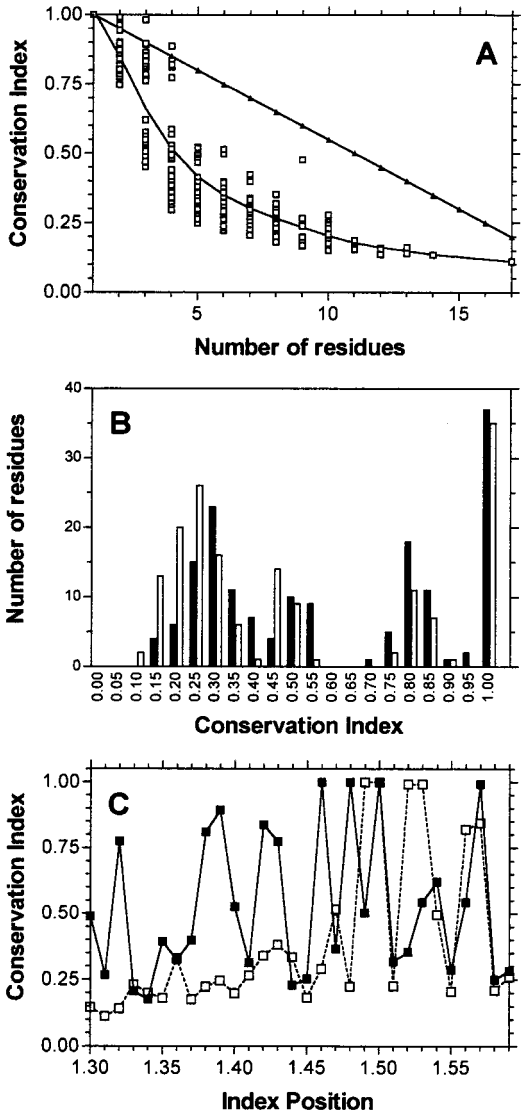


FIGURE 3: Sequence conservation analysis. (A) Comparison of the new method of calculating conservation index (CI) (open squares) (see Experimental Procedures) with the method of counting the number of residues present at each position (solid triangles). The results of the new method were calculated from the conservation indices of all the transmembrane residues in both rMA and cMA. The curve is the result of coarse LOWESS fitting (GraphPad Prism) of the average CIs for each number of residues. (B) Comparison of the distribution of CIs in TM2−TM7 of rMA (solid bars) and cMA (open bars) showing a similar overall degree of sequence conservation. (C) The CIs of TM1 (1.30−1.59) of rMA (solid squares) and cMA (open squares).

conserved proline at position 1.48. In the bovine rhodopsin structure, this proline causes a 10° kink in TM1 [calculated according to (*31*)], which makes the extracellular portion of TM1 bend toward the interior of the transmembrane bundle (*9*). In catecholamine receptors, there is no proline at position 1.48 but rather a highly conserved glycine at 1.49, and, TM1, given the absence of a proline kink, may be straighter and possibly more exposed to the lipid milieu.

We created a multiple sequence alignment of 101 opsins with Pro at 1.48 (rMA) and another of 104 catecholamine receptors with Gly at 1.49 (cMA), and we analyzed the conservation of each position in these alignments using a novel measure of conservation (see Experimental Procedures). The method of simply counting the number of

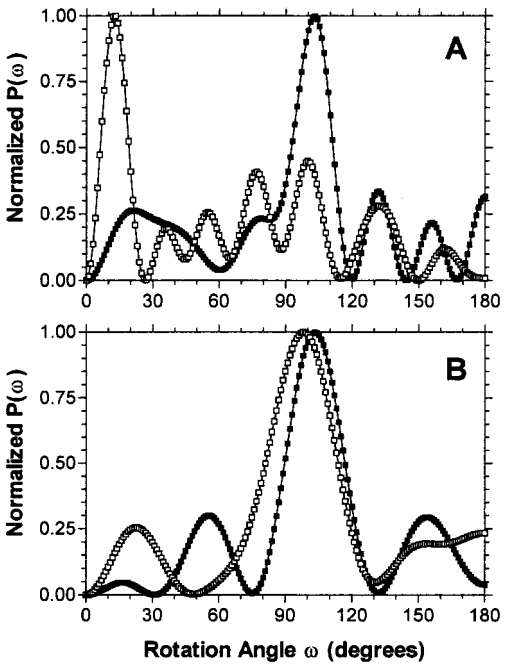


FIGURE 4: Fourier transform analysis of sequence conservation indices of rMA (solid squares) and cMA (open squares) in the segments 1.30−1.47 (A) and 1.50−1.59 (B). Calculations were performed as described under Experimental Procedures.

different amino acids (AAs) present at each position (*25*) produces a linear relationship between the number of residues at a position and the conservation index (CI) (Figure 3A). It seems apparent, however, that the decrease in the degree of conservation in going from 19 to 20 residues at a given position should be much less than, for example, going from 1 to 2 residues. In contrast to a linear relationship, our method of calculation produces a smaller incremental decrease in CI for each additional residue at a given position as the number of residues increases (Figure 3A). Such a pattern is also consistent with the probability distribution of information using entropy as the measure. To illustrate, given the entropy ($-n \times {}^1/_n \times \log_2 {}^1/_n$) for a number of equally distributed residues at a position (*32*), the change in entropy, $\log_2 ({}^1/_k + 1)$, is smaller for each incremental increase in the number of residues (from $k$ to $k + 1$). Furthermore, in addition to the number of residues, our method also weights the likelihood of particular AA substitutions, as well as the frequency distribution.

Figure 3B shows that rMA and cMA share a similar degree of overall sequence conservation and variation in the transmembrane domains from TM2−TM7. In the conservation analysis of TM1 of rMA (Figure 3C), several residues in the extracellular portion of TM1 are highly conserved, consistent with the existence of key contacts, presumably due to the inward bend caused by Pro$^{1.48}$. In contrast, analysis of the extracellular portion of TM1 in cMA shows no highly conserved residues, consistent with the absence of critical contacts.

Fourier transform analysis characterizes quantitatively the periodicity of conserved and variable residues in a MA according to their variability profiles. Because the degree of sequence conservation at a given position is inversely correlated with the degree of solvent exposure, α-helices on the surface of proteins are expected to show an α-helical

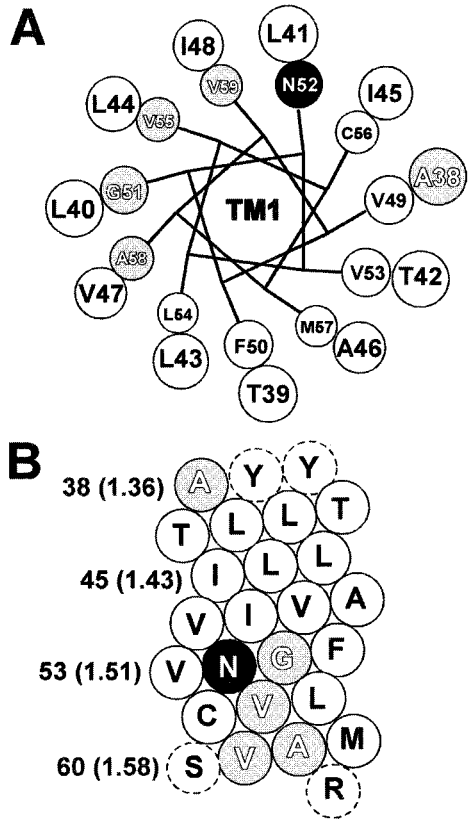


FIGURE 5: Helical wheel (A) and helical net (B) representations of the residues in the TM1 of the dopamine D2 receptor, summarizing the effects of MTSEA and MTSHTEA on [$^3$H]*N*-methylspiperone binding. Open circles indicate that these reagents had no significant effect on binding. Shaded circles indicate that MTSEA and/or MTSHTEA significantly inhibited binding. The black circles indicate the sulpiride-protected residue. Dashed circles indicate residues not mutated. In (A), increasing sizes of the circles indicate increasingly extracellular localization of the indicated residues.

periodicity in their conservation pattern (*24*, *25*). We analyzed the extent of α-helical periodicity of the conservation pattern quantified by the conservation index (CI) of the extracellular region (1.30−1.47) and intracellular region (1.50−1.59) of TM1 from the rMA and cMA (Figure 4). The analysis of the extracellular portion of TM1 (Figure 4A) gave a $\Psi = 2.6$ for the opsins. In contrast, the corresponding analysis for the catecholamine receptors gave a $\Psi = 1.0$. A $\Psi$ greater than 2 suggests a strong tendency for a segment to be α-helical (*25*). Low $\Psi$ does not necessarily mean that a segment is not α-helical, as it is possible that most of the residues within such a segment are in the core region of the protein, surrounded by conserved contacts and thus with a uniformly high CI, or that the residues are in contact with solvent, in our case the lipid bilayer, and thus with a uniformly low CI.

The overall conservation of the cytoplasmic portion of TM1 of the opsins is similar to that of the extracellular portion (Figure 3C). In contrast, the conservation of the cytoplasmic portion of TM1 of the catecholamine receptors is much greater than the conservation of the extracellular portion, and comparable to that of TM1 of the opsins. The residues conserved among the catecholamine receptors include the completely conserved Asn$^{1.50}$, the highly conserved Gly$^{1.49}$ and Val$^{1.52}$, and the $\beta$-branched (Val, Ile) conserved 1.53 and 1.57. The Fourier transform analysis of

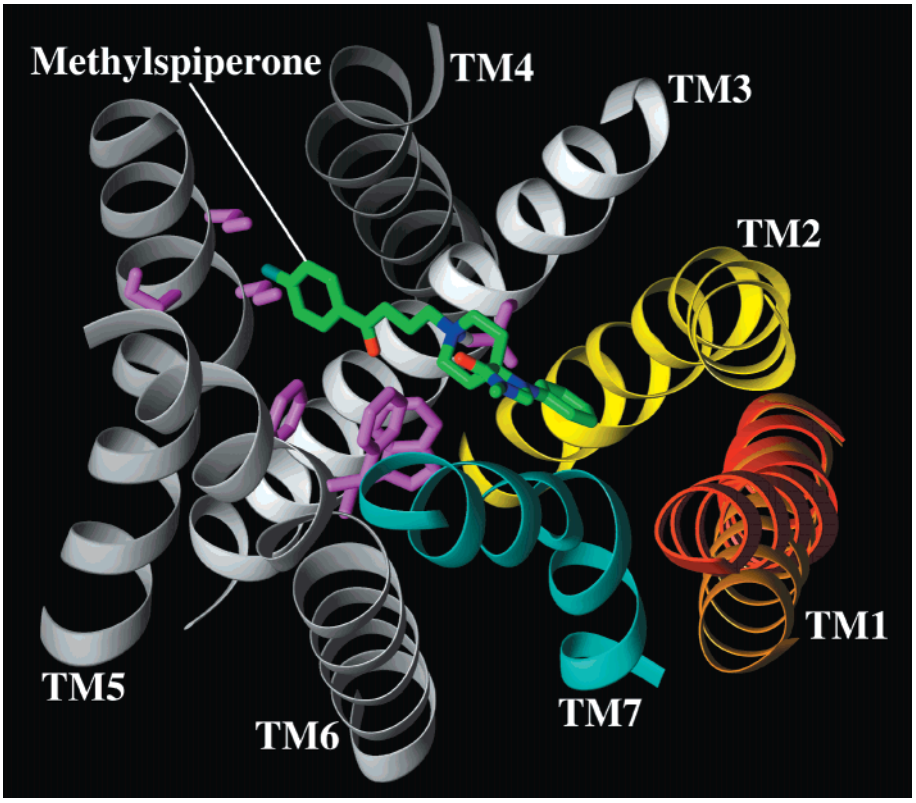


FIGURE 6: 3D molecular representations of the transmembrane domain of the human dopamine D2 receptor model, viewed extracellularly. The Cα ribbons of TM1, TM2, and TM7 of the D2 receptor model are shown in orange, yellow, and blue, respectively. The other TMs are shown in gray. The model was superimposed on the conserved cytoplasmic portion of the bovine rhodopsin structure (*9*). The TM1 Cα ribbon of bovine rhodopsin is shown in bright orange. A molecule of methylspiperone was manually docked within the binding-site crevice, attempting to maximize contacts near key residues previously found to be important in ligand binding ($Asp^{3.32}$, $Ser^{5.42}$, $Ser^{5.43}$, $Ser^{5.46}$, $Trp^{6.48}$, $Phe^{6.51}$, and $Phe^{6.52}$, all shown as purple sticks).

this region in the catecholamine receptors also revealed a periodicity consistent with α-helical character ($\Psi = 2.8$), comparable to that of the opsins ($\Psi = 3.3$) (Figure 4B).

## DISCUSSION

*Residues Forming the Water-Accessible Surface of the Binding-Site Crevice*. We identify residues on the water-accessible surface of the D2 receptor by the ability of the MTS reagents to react with substituted cysteine residues. The MTS reagents react $>10^9$ times faster with ionized thiolates than with un-ionized thiols (*33*), and only water-accessible cysteines are likely to ionize to a significant extent. Moreover, MTSEA, MTSET, and MTSES are charged and hydrophilic (*10*). Thus, we assume that these reagents will react much faster with water-accessible cysteine residues than with cysteines facing the protein interior or lipid. Based on the near-normal affinities of the cysteine mutants for *N*-methylspiperone, it is likely that the global structures of the mutants are near normal and that the substituted cysteines are reliable reporters for the accessibility of the wild-type residue for which they are substituted. We infer that the MTS reagents have reacted if the binding of ligand is irreversibly affected. Thus, although the mechanism could be steric, electrostatic, or indirect, a change in binding is taken as evidence for reaction.

SCAM relies upon an indirect assessment of accessibility based on the effects of reaction of MTS derivatives on function, in this case ligand binding. Since TM1 is the most remote TM from the binding-site crevice, it is possible that reaction takes place at positions in TM1 without affecting binding, thereby resulting in a false negative conclusion about accessibility. Indeed the bulkier MTSHTEA did appear to react with $V55^{1.53}C$, suggesting the possibility of a silent reaction of this substituted Cys with MTSEA, MTSET, and MTSES.

Based on the overall results with the 4 sulfhydryl reagents, we infer that 6 of the 21 residues tested are on the water-accessible surface of the D2 receptor. These include: $A38^{1.36}C$, $G51^{1.49}C$, $N52^{1.50}C$, $V55^{1.53}C$, $A58^{1.56}C$, and $V59^{1.57}C$ (Figure 5). All of these mutants reacted with MTSEA, except for $V55^{1.53}C$ (Figure 1). The negatively charged MTSES reacted with a subset of the residues that reacted with MTSEA, $G51^{1.49}C$, $N52^{1.50}C$, and $V59^{1.57}C$. Although reaction did not reach statistical significance for the positively charged MTSET, the overall results were similar to those with MTSES (Figure 2). MTSHTEA reacted with $N52^{1.50}C$ and $V55^{1.53}C$. Spin-labeling studies of rhodopsin that identified positions 1.56 and 1.57 as facing the protein interior and positions 1.54, 1.55, 1.58, and 1.59 as facing lipid (*34*) are consistent with the SCAM results.

The two mutants for which we were able to determine rates of reaction with MTSEA, $N52^{1.50}C$ and $V59^{1.57}C$, reacted much more slowly than accessible residues in the other TMs at similar depth within the transmembrane domain. The slow rates may reflect intermittent accessibility of these substituted Cys in TM1, which may result from dynamic structural fluctuations at the TM1−TM2−TM7 interface, relatively deep into the transmembrane domain and

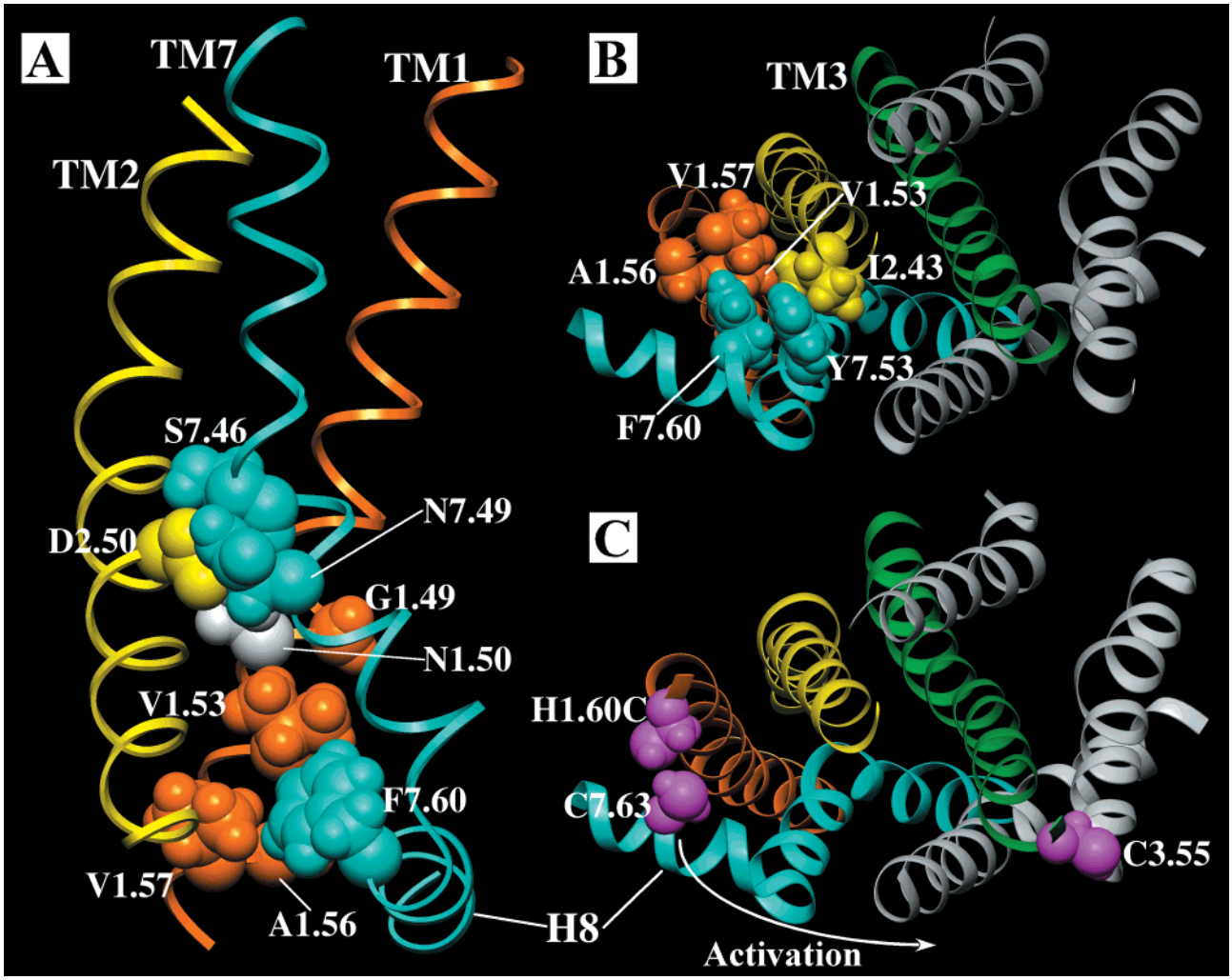


FIGURE 7: Interactions of TM1−TM2−TM7−H8. The color scheme of the ribbons is the same as that in Figure 6, except for TM3, which is shown in green. All residues are the same color as the ribbons in which they are located, except for the protected Asn$^{1.50}$, which is shown in white. (A) Side view of TM1, TM2, and TM7, clustered together by the interhelical hydrogen-bond (H-bond) network that includes Asn$^{1.50}$, Asp$^{2.50}$, Ser$^{7.46}$, and Asn$^{7.49}$. The top of the panel is the extracellular side. The accessible residues in TM1 are primarily located immediately below the H-bond network (except for Ala$^{1.36}$, which is not shown) where the Asn$^{7.49}$-Pro$^{7.50}$ kink bends TM7 away from the cluster and opens a cleft toward TM1. Phe$^{7.60}$ in H8 interacts with the accessible residues at the cytoplasmic end of TM1 (Val$^{1.53}$, Ala$^{1.56}$, and Val$^{1.57}$) (see Discussion). (B) The D2 receptor model viewed from the intracellular side. Tyr$^{7.53}$ and Phe$^{7.60}$ are stacked in the grooves formed by Val$^{1.53}$, Ala$^{1.56}$/Val$^{1.57}$, and Ile$^{2.43}$ (see Discussion). (C) The inactive-state rhodopsin structure (*9*) viewed from the intracellular side, from the same angle as in (B), showing proximity between a Cys substituted for His65$^{1.60}$ and Cys316$^{7.63}$ (shown in purple) (*38*). Cys316$^{7.63}$ can form a disulfide bond with Cys140$^{3.55}$ (shown in purple) in the active state (*39*), and this requires a large conformational change, indicated by the arrow showing the direction of proposed movement of H8 during activation.

away from identified ligand−receptor contact sites. Given the large distance between Asn52$^{1.50}$ and bound ligand, it is likely that the partial protection of N52$^{1.50}$C by sulpiride results from a retardation of access of MTSEA through the binding-site crevice to this substituted cysteine and/or sulpiride stabilization of the conformation of the receptor and decrease in the structural fluctuations that may facilitate reaction. Thus, although according to our definition Asn52$^{1.50}$ is part of the binding-site crevice, modification of this position, as well as the patch of residues located below this position, likely inhibits binding through an indirect mechanism. Given the role we postulate for some of these residues in stabilizing the TM1−TM7−H8 interface (see below), mutation of some of these residues to cysteine, although without significant impact on ligand binding, may increase local structural fluctuations and facilitate access of MTSEA.

*The Secondary and Tertiary Structure of TM1*. The pattern of accessibility is consistent with an α-helical conformation at the intracellular part of TM1 (from G51$^{1.49}$C to V59$^{1.57}$C) (Figure 5). Other than A38$^{1.36}$C, MTSEA had no effect on binding on any mutant more extracellular than G51$^{1.49}$C. Unlike rhodopsin, the D2 receptor does not contain a Pro at position 1.48, and TM1 is not expected to be kinked in the D2 receptor as it is in rhodopsin (*9*). The absence of a substantial kink in the D2 receptor would position the extracellular portion of TM1 further away from TM2 and TM7 than in rhodopsin, and thus more exposed to the lipid milieu. Such a positioning, illustrated in Figure 6, is consistent with the SCAM results as well as with our analysis showing poor conservation of the extracellular portion of TM1 in catecholamine receptors (Figure 3C), with the lack of key contacts in this region, and with the generally minimal effect of mutations in this region of catecholamine receptors. The conserved Gly at position 1.49 may allow flexibility and/or bending (*30*), consistent with the results of our molecular dynamics simulations, in which the presence of a

Gly produced on average bend of 5° in a model α-helix. Thus, it is possible that some bend in TM1 of catecholamine receptors may occur even without Pro$^{1.48}$ and/or that the extracellular portion of TM1 in catecholamine receptors is significantly more dynamic than the aligned region in rhodopsin.

In the rhodopsin structure, the highly conserved Asn55$^{1.50}$ is hydrogen bonded to Asp83$^{2.50}$ and to the backbone carbonyl of Ala299$^{7.46}$ in TM7; Asp83$^{2.50}$ is also in contact with Asn302$^{7.49}$ (*9*, *35*). On the basis of site-directed mutagenesis experiments, the highly conserved Asn$^{1.50}$ has been proposed to be part of a "polar pocket" that also includes Asp$^{2.50}$, Asn$^{7.49}$, and Tyr$^{7.53}$ (*36*). In the rhodopsin structure, Gly54$^{1.49}$ and Asn55$^{1.50}$ in TM1 are predicted to be accessible in the binding-site crevice near the interface of TM1 with TM2 and TM7 (Figure 7A). Due to the bend in TM7 generated by the Asn-Pro kink below these contact points, the intracellular portion of TM1 might be accessible to MTSEA from the binding-site crevice (Figure 7A). The residues at 1.53 and 1.57 are highly conserved as $\beta$-branched residues (Val and Ile in catecholamine receptors, and Val and Thr in opsins). The side chains of $\beta$-branched residues in α-helices are conformationally constrained (*37*). These residues were accessible in the D2 receptor, as was 1.56 (Figure 5). Several residues in TM7 and H8 face into the interior of the transmembrane bundle and are highly conserved, including 7.53, 7.60, and 7.64. In our D2 receptor model, as in rhodopsin, Tyr$^{7.53}$ and Phe$^{7.60}$ stack together and fit into two grooves, with 7.53 between 1.53/1.57 and 2.43 (conserved in catecholamine receptors and in opsins as $\beta$-branched Val or Ile, as well as bulky Leu), and 7.60 between 1.56 and 1.53/1.57 (Figure 7B). We propose that these interactions play an important role in stabilizing the inactive state of the receptor and the position of H8.

In the inactive state of rhodopsin, Cys$^{1.60}$ (substituted for His) and Cys$^{7.63}$ were found to be in proximity based on disulfide formation and interaction between attached spin-labels (*38*). These two residues are in close contact (3.0 Å) in the bovine rhodopsin structure, which represents the inactive state (*9*)(Figure 7C). In the light, Cys$^{7.63}$ can disulfide bond to Cys$^{3.55}$ (*39*). The distance between these residues in the inactive state of bovine rhodopsin is 26 Å (Figure 7C). Although it is conceivable that the disulfide formation traps rare conformations that result from increased dynamic fluctuations in the active state, it seems more likely that the change in cross-linking results from a more coordinated conformational rearrangement that involves a large activation-associated movement of TM7−H8. Consistent with this interpretation, an epitope at the cytoplasmic end of TM7 (7.51−7.58) of rhodopsin becomes accessible to a monoclonal antibody during activation (*40*). Moreover, whereas 7.60 interacts with TM1 in the inactive state, the N-terminal portion of H8, including 7.60, has been inferred to interact with transducin upon receptor activation (*41*), which would also require significant conformational change.

Cys$^{7.69}$ and Cys$^{7.70}$ in rhodopsin are palmitoylated and expected to interact with the membrane (*42*, *43*) and presumably help to stabilize the orientation of H8. Depalmitoylation increased the ability of rhodopsin to activate transducin (*44*). In the $\beta_2$ adrenergic receptor, activation appears to result in the rapid depalmitoylation of Cys341$^{7.69}$ (*45*). We propose that the activation-induced loss of palmitoylation weakens the association of H8 with the membrane, thereby allowing a significant conformational change in the TM7−H8 region that disrupts the stabilizing interactions with TM1 and TM2. Consistent with this hypothesis, upon photoactivation of rhodopsin, spin-labels attached to 7.61 and 7.64 reported increased mobility (*46*, *47*), and 7.64 was inferred to move away from 1.60 (*38*). Thus, in addition to interactions between the cytoplasmic ends of TM3 and of TM6 (*48*), this scheme of TM1−TM7−H8 and H8−lipid interactions may be a common mechanism for stabilizing GPCRs in the inactive state.

## ACKNOWLEDGMENT

We thank Drs. Olivier Civelli, Brian Kobilka, and Steve Rees for the human D2 receptor cDNA, epitope-tagged $\beta_2$ adrenergic receptor cDNA (used to make the epitope-tagged D2 receptor cDNA), and the pcin4 vector, respectively. We thank Irache Visiers and Harel Weinstein for helpful discussion.

## REFERENCES

1. Strader, C. D., Fong, T. M., Tota, M. R., Underwood, D., and Dixon, R. A. (1994) *Annu. Rev. Biochem. 63*, 101−132.
2. Unger, V. M., Hargrave, P. A., Baldwin, J. M., and Schertler, G. F. (1997) *Nature 389*, 203−206.
3. Visiers, I., Ballesteros, J. A., and Weinstein, H. (2001) *Methods Enzymol.* (in press).
4. Ballesteros, J., and Weinstein, H. (1995) *Methods Neurosci. 25*, 366−428.
5. Baldwin, J. M., Schertler, G. F., and Unger, V. M. (1997) *J. Mol. Biol. 272*, 144−164.
6. Kristiansen, K., Dahl, S. G., and Edvardsen, O. (1996) *Proteins: Struct., Funct., Genet. 26*, 81−94.
7. Ling, K., Wang, P., Zhao, J., Wu, Y. L., Cheng, Z. J., Wu, G. X., Hu, W., Ma, L., and Pei, G. (1999) *Proc. Natl. Acad. Sci. U.S.A. 96*, 7922−7927.
8. Quitterer, U., Zaki, E., and AbdAlla, S. (1999) *J. Biol. Chem. 274*, 14773−14778.
9. Palczewski, K., Kumasaka, T., Hori, T., Behnke, C. A., Motoshima, H., Fox, B. A., Le Trong, I., Teller, D. C., Okada, T., Stenkamp, R. E., Yamamoto, M., and Miyano, M. (2000) *Science 289*, 739−745.
10. Karlin, A., and Akabas, M. H. (1998) *Methods Enzymol. 293*, 123−145.
11. Akabas, M. H., Stauffer, D. A., Xu, M., and Karlin, A. (1992) *Science 258*, 307−310.
12. Javitch, J. A., Shi, L., Simpson, M. M., Chen, J., Chiappa, V., Visiers, I., Weinstein, H., and Ballesteros, J. A. (2000) *Biochemistry 39*, 12190−12199.
13. Javitch, J. A., Ballesteros, J. A., Chen, J., Chiappa, V., and Simpson, M. M. (1999) *Biochemistry 38*, 7961−7968.
14. Javitch, J. A., Ballesteros, J. A., Weinstein, H., and Chen, J. (1998) *Biochemistry 37*, 998−1006.
15. Fu, D., Ballesteros, J. A., Weinstein, H., Chen, J., and Javitch, J. A. (1996) *Biochemistry 35*, 11278−11285.
16. Javitch, J. A., Fu, D., and Chen, J. (1995) *Biochemistry 34*, 16433−16439.
17. Javitch, J. A., Fu, D., Chen, J., and Karlin, A. (1995) *Neuron 14*, 825−831.
18. Javitch, J. A., Li, X., Kaback, J., and Karlin, A. (1994) *Proc. Natl. Acad. Sci. U.S.A. 91*, 10355−10359.
19. Stauffer, D. A., and Karlin, A. (1994) *Biochemistry 33*, 6840−6849.
20. Rees, S., Coote, J., Stables, J., Goodson, S., Harris, S., and Lee, M. G. (1996) *BioTechniques 20*, 102−110.
21. Blumenthal, L. M. (1970) Theory and Applications of Distance Geometry pp 97−99, Chelsea Publishing Co., Bronx, New York.

22. Overington, J., Donnelly, D., Johnson, M. S., Sali, A., and Blundell, T. L. (1992) *Protein Sci. 1*, 216−226.
23. Gorodkin, J., Heyer, L. J., Brunak, S., and Stormo, G. D. (1997) *Comput. Appl. Biosci. 13*, 583−586.
24. Donnelly, D., Overington, J. P., and Blundell, T. L. (1994) *Protein Eng. 7*, 645−653.
25. Rees, D. C., Komiya, H., Yeates, T. O., Allen, J. P., and Feher, G. (1989) *Annu. Rev. Biochem. 58*, 607−633.
26. Cornette, J. L., Cease, K. B., Margalit, H., Spouge, J. L., Berzofsky, J. A., and DeLisi, C. (1987) *J. Mol. Biol. 195*, 659−685.
27. Ballesteros, J. A., Shi, L., and Javitch, J. A. (2001) *Mol. Pharmacol. 60*, 1−19.
28. Bower, M. J., Cohen, F. E., and Dunbrack, R. L. (1997) *J. Mol. Biol. 267*, 1268−1282.
29. Brooks, B. R., Bruccoleri, R. E., Olafson, B. D., States, D. J., Swaminathan, S., and Karplus, M. (1983) *J. Comput. Chem. 4*, 187−217.
30. Kumar, S., and Bansal, M. (1998) *Biophys. J. 75*, 1935−1944.
31. Visiers, I., Braunheim, B. B., and Weinstein, H. (2000) *Protein Eng. 13*, 603−606.
32. Weiss, O., Jimenez-Montano, M. A., and Herzel, H. (2000) *J. Theor. Biol. 206*, 379−386.
33. Roberts, D. D., Lewis, S. D., Ballou, D. P., Olson, S. T., and Shafer, J. A. (1986) *Biochemistry 25*, 5595−5601.
34. Altenbach, C., Klein-Seetharaman, J., Hwa, J., Khorana, H. G., and Hubbell, W. L. (1999) *Biochemistry 38*, 7945−7949.
35. Menon, S. T., Han, M., and Sakmar, T. P. (2001) *Physiol. Rev.* (in press).
36. Scheer, A., Fanelli, F., Costa, T., De Benedetti, P. G., and Cotecchia, S. (1996) *EMBO J. 15*, 3566−3578.
37. Piela, L., Nemethy, G., and Scheraga, H. A. (1987) *Biopolymers 26*, 1273−1286.
38. Yang, K., Farrens, D. L., Altenbach, C., Farahbakhsh, Z. T., Hubbell, W. L., and Khorana, H. G. (1996) *Biochemistry 35*, 14040−14046.
39. Yu, H., Kono, M., and Oprian, D. D. (1999) *Biochemistry 38*, 12028−12032.
40. Abdulaev, N. G., and Ridge, K. D. (1998) *Proc. Natl. Acad. Sci. U.S.A. 95*, 12854−12859.
41. Marin, E. P., Krishna, A. G., Zvyaga, T. A., Isele, J., Siebert, F., and Sakmar, T. P. (2000) *J. Biol. Chem. 275*, 1930−1936.
42. Ovchinnikov, Y. A., Abdulaev, N. G., and Bogachuk, A. S. (1988) *FEBS Lett. 230*, 1−5.
43. Papac, D. I., Thornburg, K. R., Bullesbach, E. E., Crouch, R. K., and Knapp, D. R. (1992) *J. Biol. Chem. 267*, 16889−16894.
44. Morrison, D. F., O'Brien, P. J., and Pepperberg, D. R. (1991) *J. Biol. Chem. 266*, 20118−20123.
45. Loisel, T. P., Ansanay, H., Adam, L., Marullo, S., Seifert, R., Lagace, M., and Bouvier, M. (1999) *J. Biol. Chem. 274*, 31014−31019.
46. Altenbach, C., Cai, K., Khorana, H. G., and Hubbell, W. L. (1999) *Biochemistry 38*, 7931−7937.
47. Resek, J. F., Farahbakhsh, Z. T., Hubbell, W. L., and Khorana, H. G. (1993) *Biochemistry 32*, 12025−12032.
48. Ballesteros, J. A., Jensen, A. D., Liapakis, G., Rasmussen, S. G., Shi, L., Gether, U., and Javitch, J. A. (2001) *J. Biol. Chem. 276*, 29171−29177.

BI011204A